

## **RAMAN SCATTERING FROM SEMICONDUCTOR NANOPARTICLES AND SUPERLATTICES**

D. Nesheva\*

Institute of Solid State Physics, Bulgarian Academy of Sciences, 72 Tzarigradsko Chaussee Blvd., 1784 Sofia, Bulgaria

The effect of reduced dimensionality on the shape and position of the first order phonon bands in the Raman scattering spectrum of semiconductors is described. Off-resonance and resonance Raman scattering from semiconductor nanoparticles and superlattices are then considered. Results on nanocrystal size determination, lattice ordering and crystallization of amorphous ultra-thin films, interface induced stress, phase separation of supersaturated solid solutions, interface alloying and the electronic structure are presented.

(Received December 9, 2004; accepted January 26, 2005)

*Keywords:* Raman scattering, Nanoparticles, Ultra-thin films, Superlattice

### **1. Introduction**

The optical and vibrational properties of low-dimensional semiconductors attract much interest, because they differ significantly from those of corresponding bulk materials and offer a great variety of attractive applications in electronic, optoelectronic and optical devices, solar cells, sensors etc. In order to get information about these properties, a number of techniques developed for bulk materials (infra red and visible absorption, Raman scattering, photoluminescence, photocurrent measurements, etc.) are applied, as new theoretical considerations have been carried out taking into account the reduced dimensionality of nanosized materials.

The Raman scattering (RS) technique, based on inelastic light scattering, is a well established procedure for the fast and non-destructive measurement of stress, crystal lattice disorder and homogeneity of materials with up to ~100 nm spatial resolution. Being sensitive to the crystal potential fluctuations and local atomic arrangement, RS is an excellent probe for studying nanostructured materials. The phonon bands appearing in the first order Raman spectrum of a macroscopic crystal have a Lorentzian line shape. Disorder and particle size change the shapes and positions of Raman lines. This make it possible, in addition to the rich information taken for bulk materials, to obtain data about nanoparticle size, shape and size distribution etc.

In this article, the size-induced changes in the Raman spectrum of semiconductors are considered, and a variety of applications of the RS technique to nanostructures containing semiconductor nanoparticles or ultra-thin films are described

### **2. Photon-phonon interactions**

Light scattering in homogeneous materials is due to dynamic inhomogeneities in their dielectric constant, related to the acoustic or optical wave propagation i.e. fluctuations in the internal mechanical strain. These fluctuations cause inelastic scattering of light, and a change in its

---

\* Corresponding author: nesheva@issp.bas.bg

frequency. The two most typical cases of the inelastic scattering in crystalline materials are: Brillouin scattering (from acoustic phonons) and Raman scattering (from optical phonons).

The scattering phenomena are two-photon processes, in which an incident photon is momentarily absorbed into a virtual state. A new photon is created and scattered from this virtual level. The final state can be either the vibrational ground state (this gives Rayleigh scattering) or the vibrational excited state (giving Stokes-Raman scattering). In the Stokes-Raman scattering process (Fig.1) a photon with energy  $\hbar\omega_i$  transfers a part of this energy to the lattice, thus creating a phonon with energy  $\hbar\omega_o$  which leaves the interaction region with a lower energy.

$$\hbar\omega_{s1} = \hbar\omega_i - \hbar\omega_o . \quad (1)$$

The scattering process can also originate from the vibrationally excited state and proceed via the virtual state to the vibrational ground state. This process is known as anti-Stokes-Raman scattering. In this case, the scattered photon has energy

$$\hbar\omega_{s1} = \hbar\omega_i + \hbar\omega_o . \quad (2)$$

The described spontaneous Raman effect is an off-resonance effect. Its description requires the assumption of a virtual state, which is not intuitively obvious. It is usually considered that the lattice polarizability creates this virtual state that allows the incident light to interact with matter though there is no stationary state nearby into which photons can be absorbed. The polarizability changes make it possible for a photon of any wavelength to be absorbed.

The emitted phonon can be absorbed again by the crystal lattice, and thus a second order Raman scattering can occur. The energy of the emitted photon is

$$\hbar\omega_{s2} = \hbar\omega_{s1} - \hbar\omega_o = \hbar\omega_{si} - 2\hbar\omega_o \quad (3)$$

Such a cascade process can be repeated many times, but with increasing order of the scattering process the intensity of the scattered light strongly decreases.

### 3. Raman scattering from nanosized materials

#### 3.1 Effects of nanomaterial size and shape on the Raman spectra

In the Raman scattering process in bulk materials, both the energy and wave vector  $k$  are conserved. The value of  $k = 2\pi/\lambda$  ( $\lambda$  = wavelength) for the photons is very small when compared with the phonon wave vector  $k = 2\pi/a$  ( $a$  = lattice constant). Since two photons and one phonon participate in the scattering process, the  $k$  of the emitted phonon, which is the vector sum of the wave vectors of the photons, is also very small. This means that only phonons with  $k \approx 0$  take part in the Raman scattering process. The same is valid for Brillouin scattering. In crystalline materials, the  $k$  conservation results in a single phonon line having a Lorentzian shape and a natural line width of around  $3.5 \text{ cm}^{-1}$ .

The presence of disorder in crystalline solids (amorphization or reduced dimensionality) modifies the wave vector selection rules for optical processes. Generally, in the case of nanosized materials characterized with dimensions comparable with phonon wavelength, the description of the elementary lattice excitons with plane waves is no longer justified. A wave packet whose spatial dimension is comparable to the crystallite size is used whose confinement introduces a spread or uncertainty in wave vectors and phonons with  $k \neq 0$  can be involved in Raman scattering. This uncertainty is larger for smaller sizes of the ordered domains because the wave packet becomes more localized in real space. As the optical phonon dispersion curves are in general not flat new frequencies are introduced in the Raman spectra when contribution from phonons with significantly different wave vectors starts to play a role [1-4]. Assuming that the size reduction relaxes the Raman selection rules but does not significantly modify the phonon dispersion curves of the reference three-dimensional (3D) system, Raman lines will "red" shift and asymmetrically broaden to the low-energy side of the Raman band (see Fig.2). The nature of the changes and the crystal size at which

these changes take place depend on the dispersion curve of the material, and also on the intrinsic phonon lifetime. Normally the smaller the size, the stronger the band asymmetry.

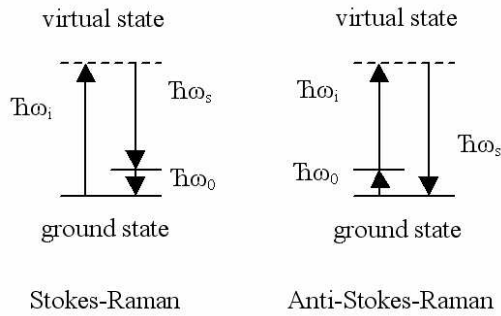


Fig. 1. Energy conservation for photon-phonon inelastic scattering with emission (left) and absorption (right) of a phonon.

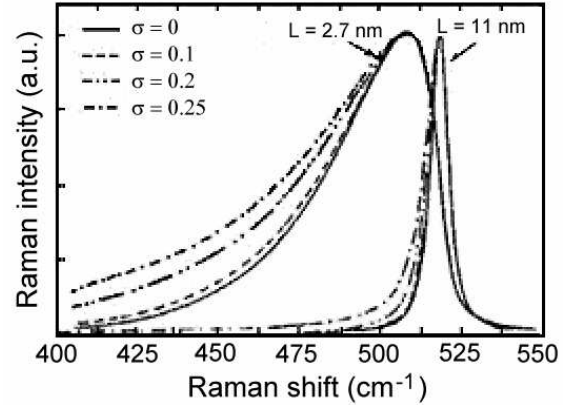


Fig. 2. Effect of nanoparticle size and variation in size distribution  $\sigma$  on the shape of the calculated Raman band from an ensemble of Si nanocrystals with two different average sizes [1].

Fig. 2 demonstrates the effect of variations of nanoparticle size and size distribution  $\sigma$  (half width at half maximum, divided by the average nanocrystal size) on the shape of the calculated Raman band of an ensemble of Si nanocrystals. It is seen that the size decrease causes a red shift of the Raman band. With increasing  $\sigma$ , the peak position keeps nearly constant, but the full width at half maximum (FWHM) of the band, as well as its asymmetry, increases significantly. Therefore, the presence of a strong and longer tail in the Raman lines can be interpreted as an indication for a broad nanoparticle size distribution. It has been calculated [1] that for large crystals ( $> 10$  nm) and/or small  $\sigma$  values ( $< 10\%$ ), the effects of  $\sigma$  variations are negligible.

Considering the phonon wave function to be partially confined to the volume of crystallites of three different shapes (thin film, column and spherical crystals, Fig. 3, left), Campbell and Fauchet [3] calculated a relationship between the FWHM/Raman shift and the crystal size (Fig. 3, right). There is a clear distinction between the spectra of the film containing many isolating spherical nanocrystals and those for the ultra thin crystalline film. The effect of the size on the position and shape of the Raman band is strongest for the spherical nanoparticles and marginal for ultra thin films. That is why, following the works of Richter *et al.* [2] and Campbell and Fauchet [3], a number of research groups have developed theoretical formalisms for calculating first order Raman scattering from nanocrystals. In those calculations, along with the effect of the reduced size of a single nanoparticle [1,5-7], the nanoparticle shape and size distribution in an ensemble of small crystals has also been considered [8]. It has been argued that for an ensemble of nanospheres, apart from superposition of the individual scattering from each single sphere, there exists a collective scattering by a coherent mode, which involves many spheres, unless their concentration is too small [8]. Several relatively simple formulas can be found in the literature, giving the intensity of the first order Raman spectrum in nanocrystals. For example, Campbell and Fauchet [3] suggested the following expression for the Raman intensity  $I$ :

$$I(\omega L) \propto \int \exp(k^2 L^2 / 2\alpha) \{d^3 k / [\alpha(k) - \omega]^2 (G_o/2)\} \quad (4)$$

where  $G_o$  is the bulk FWHM,  $\alpha(k)$  is the dispersion relation for optical phonons and  $\alpha$  is a constant representing the degree of phonon confinement. This or similar relations can be applied for determination of the average size of ensembles of small crystals by using nanocrystal size as the free parameter in a fitting procedure. It is also necessary to know or assume a function for the dispersion curve of the optical phonon [9]. Experimental Raman spectra have been used to evaluate the average

size of crystals in nanocrystalline Si and Ge films [10-12] as well as of CdS, CdSe nanocrystals embedded in various matrices [13,14].

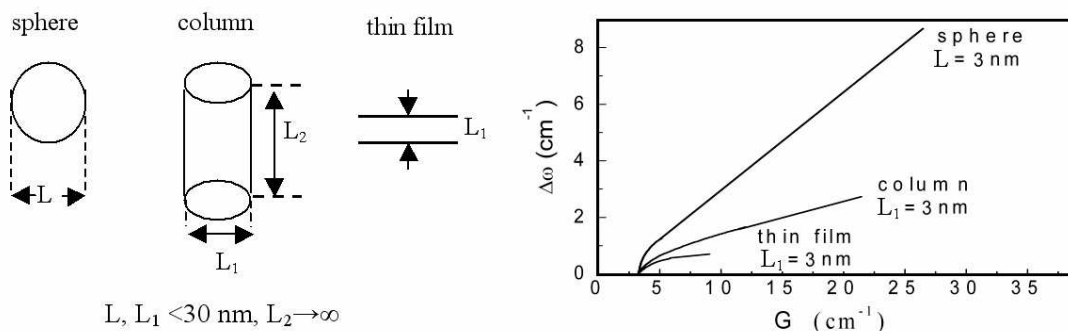


Fig. 3. Left: Zero-, one- and two-dimensional crystals. Right: Qualitative relationship between the FWHM  $G$ , shift  $\Delta\omega$  and crystal size  $L$  for these microcrystal shapes. The shift and width scales are the same for all three shapes. The maximum  $\Delta\omega$  and  $G$  in each curve corresponds to a crystal dimension of 3 nm.

### 3.2. Off-resonance Raman scattering results

The Stokes and anti-Stokes Raman scattering considered above are off-resonance optical phenomena. When absorbing photons, the system is in a virtual state corresponding to some change in its polarizability. In this case, the Raman scattering cross section is not very high. For this reason, off-resonance Raman scattering measurements require intense excitations and relatively long integration times.

Raman scattering investigations of the effects of thermal annealing and laser illumination on the structures of amorphous Se/CdSe multilayers of various sublayer thicknesses (3.5 to 10 nm) have shown [15] that after annealing, the intensity of all bands increases for all samples, implying an improvement in the interface quality. It was also observed that a gradual increase in the laser power density caused a decrease of the  $256\text{ cm}^{-1}$  band (due to amorphous Se), and a significant increase of the  $237\text{ cm}^{-1}$  band (due to crystalline Se). This indicates that crystallization of the Se layers occurs, related mainly to the thermal effects of the laser beam. From the threshold for crystallization, it was concluded that the crystallization temperature of ultra-thin Se films is significantly higher than that of bulk Se. Thus, the Raman scattering experiments confirmed the prediction of thermodynamic considerations for an increase in the crystallization temperature of 2D amorphous materials when compared to that of the 3D material.

Raman scattering measurements have been used to explore the photocrystallization of  $\text{Se}_{70}\text{Te}_{30}$  layers in  $\text{Se}/\text{Se}_{70}\text{Te}_{30}$  amorphous multilayers having various layer thicknesses [16,17]. Spectra obtained for  $\text{Se}(4\text{ nm})/\text{Se}_{70}\text{Te}_{30}$  multilayers having  $\text{Se}_{70}\text{Te}_{30}$  layer thicknesses of 3.5 and 7.0 nm are shown in Fig.4. In order to avoid heating of the samples and thermally-induced crystallization, the spectra were taken at 20 K and at a low laser beam intensity. It is seen that when exciting the sample having thinner  $\text{Se}_{70}\text{Te}_{30}$  layers with a laser beam power of  $55\text{ W}\cdot\text{cm}^{-2}$ , the  $237\text{ cm}^{-1}$  band related to crystalline Se appears after much longer illumination than in the case of the sample with thicker  $\text{Se}_{70}\text{Te}_{30}$  layers. Thus, the RS results have shown for the first time that, similarly to thermally-induced crystallization, photoinduced crystallization of ultra-thin amorphous films is strongly affected by the size reduction.

Since Raman scattering is very sensitive to the composition of materials, it can be used to check interface alloying in multilayer structures, as well as compositional homogeneity. Raman results on interface alloying in  $\text{ZnSe}/\text{CdSe}$  multilayers are shown in Fig.5. It is seen that a significant increase of the FWHM of the 1LO (longitudinal optical) band of CdSe ( $210\text{ cm}^{-1}$ ) takes place with decreasing CdSe and ZnSe layer thickness. This increase has been related [18] to the formation of  $\text{ZnCdSe}$  regions at the interfaces. The relative volume of these regions increases when the layer thickness decreases. The annealing induces a further increase of the FWHM, indicating that the total volume of the  $\text{ZnCdSe}$  regions in annealed films is appreciably greater than that in as-deposited multilayers.

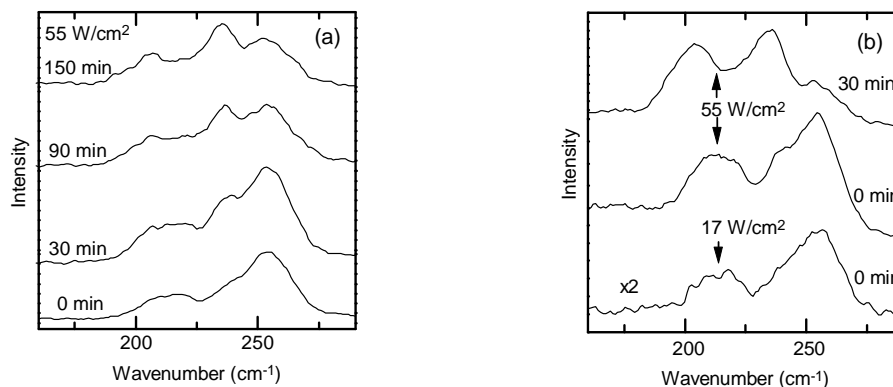


Fig. 4. Raman scattering spectra of Se(4 nm)/Se<sub>70</sub>Te<sub>30</sub> amorphous multilayers having Se<sub>70</sub>Te<sub>30</sub> sublayer thickness of: (a) - 3.5; (b) - 7.0 nm. The spectra were measured at a constant spot of each sample, after preliminary exposure to the respective laser beam power noted for each spectrum.

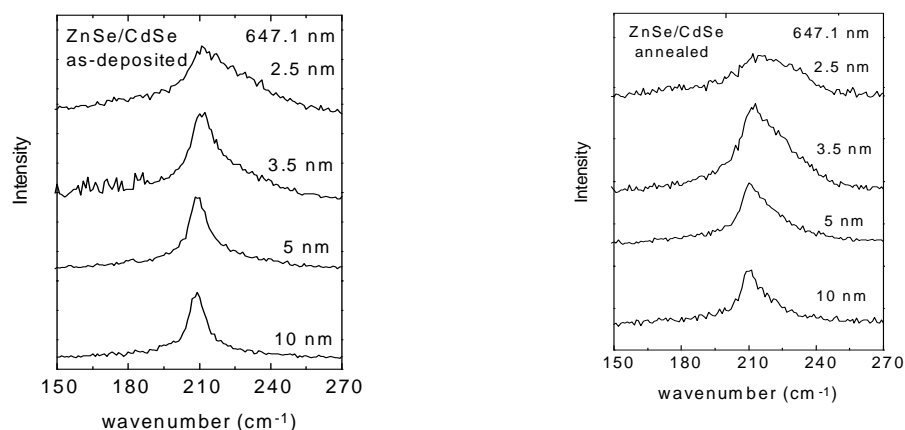


Fig. 5. Raman scattering spectra of as-deposited and annealed ZnSe/CdSe multilayers with various layer thicknesses. The ZnSe and CdSe layers have the same thickness.

Phase separation of supersaturated solid solutions is widely used for the preparation of semiconductor nanoparticles embedded in glass matrices. In general, the size distribution of the nanoparticles grown using this technique is rather broad. As discussed above, Raman scattering can give very useful information about the nanocrystal size and shape distribution. For this reason, it is frequently used to control and optimize the parameters (saturation, temperature and duration) of the nanoparticle growth process. Fig.6 shows Raman spectra of SiO<sub>x</sub> films with different oxygen contents, annealed at 523, 973 or 1303 K [19]. The spectra of samples annealed at 523 K display a narrow band that originates from the c-Si substrate, and one can conclude that no phase separation occurs upon this annealing. The spectra of samples annealed at 973 K exhibit two wide bands at  $\sim 150$  cm<sup>-1</sup> and  $\sim 480$  cm<sup>-1</sup>. These bands are typical of amorphous Si, and their appearance indicates that, at this temperature, phase separation occurs and regions of 'pure' amorphous silicon are formed. The absorption of the 488 nm light in a-Si is stronger than in SiO<sub>x</sub>. For this reason, the intensity of light scattered from the substrate is reduced. In the samples annealed at 1303 K, the 150 cm<sup>-1</sup> band was not observed. A tail of the band from the c-Si substrate, which is not as long as in the case of a-Si, is seen in Fig. 6. Also, the intensity of the scattered light from the substrate is increased. Keeping in mind that the absorption of crystalline Si is weaker than that of amorphous silicon one can infer that Si nanocrystals were grown upon annealing at 1300 K.

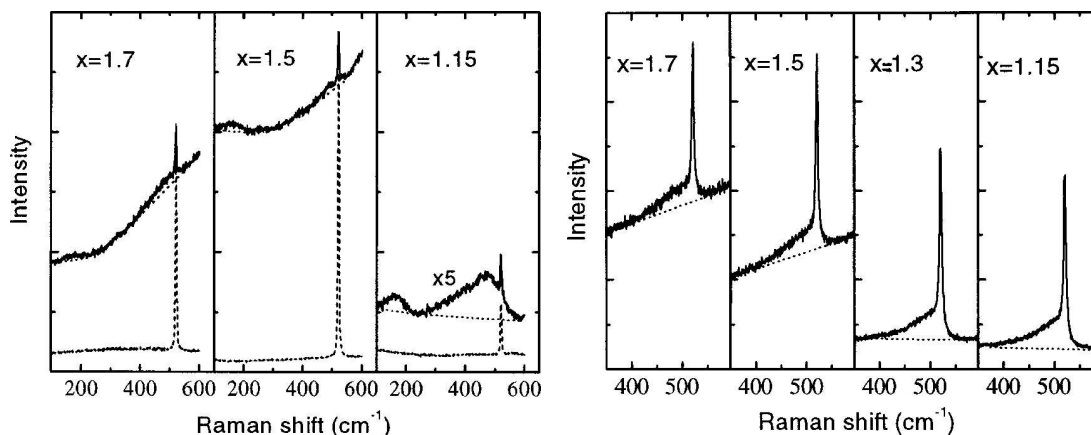


Fig. 6. Raman spectra of  $\text{SiO}_x$  films with different oxygen contents. The films were deposited on a c-Si substrate and annealed at 523 K for 30 min (left, dashed line), 973 K for 60 min (left, solid line) in argon and 1303 K for 60 min in nitrogen (right). The 488 nm  $\text{Ar}^+$  laser line was used for excitation.

Finally, in this section, we would like to mention the possibility of exploring internal strain and size-dependent lattice contraction in nanocrystals by means of the RS spectroscopy. It has been demonstrated [20] that CdSe-like and CdS-like 1LO bands of  $\text{CdS}_{1-x}\text{Se}_x$  nanocrystals embedded in a glass matrix exhibit a blue shift with respect to their positions in bulk materials. Such a shift indicates that the nanocrystals suffer compressive strain. It has been found that the strain increases as the crystallite size decreases. A model based on the cluster surface free energy on the surface-to-volume ratio has been suggested to explain the observed blue shift. Raman measurements have also been performed on CdSe nanocrystals of various sizes embedded in three different matrices ( $\text{GeO}_2$ ,  $\text{SiO}_2$ ,  $\text{B}_2\text{O}_3\text{-SiO}_2$ ) [21]. All series of samples showed the expected red shift with decreasing nanocrystal size. However, it was observed that at the same nanocrystal size the magnitude of the red shift and the band position depend on the matrix composition. The strongest shift has been registered for the  $\text{B}_2\text{O}_3\text{-SiO}_2$  series, in which an appreciable blue shift of the 1LO band of CdSe was observed in the samples with the largest nanocrystals. This result implies that the compressive strain in the  $\text{B}_2\text{O}_3\text{-SiO}_2$  samples is greater than in the other two series.

### 3.3. Resonance Raman scattering investigations

Resonance enhancement occurs in Raman spectroscopy if the energy of the exciting light is close to the energy of a stationary electronic transition of the sample. The strongest increase is normally observed when the exciting light approaches the optical band gap of the investigated material. The intensity enhancement in resonance Raman spectroscopy is very useful to study nanophase and nanostructured semiconductors, since they require measurements at small nanophase concentrations. The advantage of the resonance Raman spectroscopy is not only the increased sensitivity, but also the selectivity of the effect. It allows groups of objects (for example nanocrystals having the same size and hence the same optical band gap) to be selectively explored. The availability of lasers that can be tuned over the whole visible spectrum makes it possible to study nanocrystal size distributions, the deviation of the shape of nanocrystals from the spherical one, etc. The enhanced Raman cross section allows the observation of Raman scattering of orders higher than 3, as well as investigations of the electronic structure of nanosized semiconductors.

Raman spectra of  $\text{SiO}_x/\text{CdSe}$  multiquantum wells (MQWs) with various CdSe layer thicknesses, excited by the 647.1 nm ( $\sim 1.92$  eV)  $\text{Kr}^+$  laser line, are shown in Fig.7 [22]. The 1 LO at  $210\text{ cm}^{-1}$  and 2 LO at  $418\text{ cm}^{-1}$  phonon peaks are seen. All spectra were recorded under identical experimental conditions, and correspond to the same intensity scale. However, one can see that the Raman intensity reaches a maximum for samples with a CdSe well thickness  $\sim 3.5 - 4.0$  nm. This implies that resonant absorption takes place for these thicknesses. Hence, the optical band gap of CdSe layers is  $\sim 1.92$  eV. On the other hand, CdSe films in these MQWs are nanocrystalline. If the potential barriers between the CdSe nanocrystals are high enough and 3D confinement of charged carriers takes place in each separate nanocrystal, one can expect that their optical band gap should

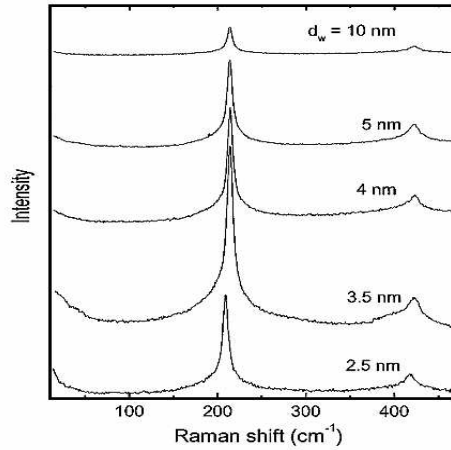


Fig. 7. Raman spectra of SiO<sub>x</sub>/CdSe multiquantum wells with various CdSe layer thicknesses, excited by the 647.1 nm Kr<sup>+</sup> laser line.

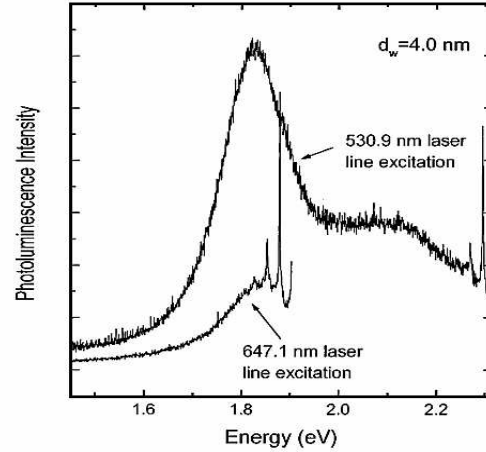


Fig. 8. Photoluminescence spectra of a SiO<sub>x</sub>/CdSe multiquantum well with a CdSe sublayer thickness of  $d_w = 4$  nm

be  $\sim 2$  eV. This discrepancy has been explained [22] by assuming low potential barriers and 1D carrier confinement that occurs in a direction perpendicular to the layer plane. Thus, the resonance RS measurements performed on SiO<sub>x</sub>/CdSe MQWs gave important information about the optical band gap of ultra-thin nanocrystalline films of CdSe and the barrier height at the grain boundaries.

Fig. 8 shows photoluminescence spectra of a SiO<sub>x</sub>/CdSe multiquantum well with a CdSe sublayer thickness of 4 nm. The sharp peaks superimposed on the luminescence spectra correspond to various orders of Raman scattering by the 1 LO phonon of CdSe. Up to five orders have been observed in the spectrum excited with the 647.1 nm laser line, while in the spectrum taken with the 530.9 nm line there are three. As discussed above, the energy of the first laser line corresponds to electron transitions between the first minibands of the valence band and conduction band. That of the second line coincides with the transition energy between the miniband of the valence band related to spin-orbit splitting and first miniband of the conduction band. It has been calculated [23] that the probability for the second transition is lower than that for the first. This may be the reason for the reduced number of Raman scattering orders observed for excitation with the 530.9 nm line, even though the absorption coefficient at this energy is higher than that for the 647.1 nm line.

Finally, we give an example of the study of higher excitons in semiconductor nanocrystals. Room temperature Raman scattering spectra of a-GeS<sub>2</sub>-CdSe composite films for four values of the average CdSe nanocrystal radius excited by the 488 and 514.5 nm Ar<sup>+</sup> laser lines are shown in Fig. 9. All spectra are normalized relative to the 343 cm<sup>-1</sup> band of the GeS<sub>2</sub> matrix. They

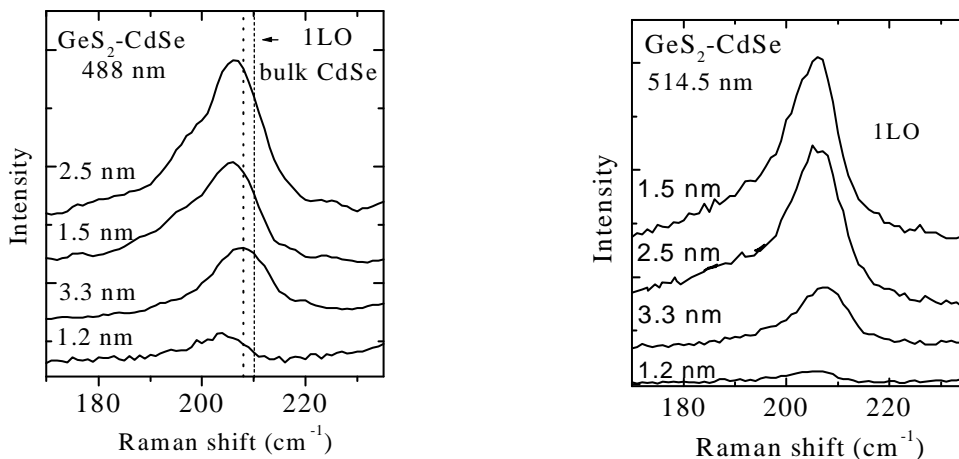


Fig. 9. Room temperature Raman scattering spectra of a-GeS<sub>2</sub>/c-CdSe composite films for four values of the average CdSe nanocrystal radius excited by the 488 nm (left) and 514.5 nm (right) Ar<sup>+</sup> laser lines.

correspond to the same intensity scale, but the observed band intensity is different. It is highest for the '2.5' nm sample with excitation by the blue line (2.54 eV) and for the '1.5 nm' sample when using the green (2.41 eV) one. This implies that resonance absorption takes place for the respective laser line. Since the energy of both lines is greater than the optical band gap of CdSe nanocrystals (2.05 eV and 2.3 eV for the '2.5' nm and '1.5 nm' samples, respectively) one can assume that resonance Raman scattering takes place for higher excitons in these nanocrystals. By variation of the measurement temperature and wavelength of the exciting light, one can get information about higher excitons in nanocrystals, which as a whole is rather scant.

#### 4. Conclusions

This review of resonance and off-resonance Raman scattering from nanosized semiconductors shows that significant changes can take place in the first order Raman band, due to sized-induced relaxation of the wave vector selection rule. The experimental data illustrate that the Raman scattering technique can be successfully applied to nanosized materials. It allows one to obtain valuable information about: interface-induced disorder in multilayers, interface alloying, crystallization of ultra thin amorphous films, phase separation in supersaturated solutions, the presence of amorphous and crystalline phases in nanostructured materials, nanocrystal size and shape, and lattice contraction. Resonance Raman scattering allows one to obtain more reliable results, and to investigate the electronic structure of low-dimensional semiconductors.

#### References

- [1] Md. N. Islam, S. Kumar, *Appl. Phys. Lett.* **78**, 715 (2001).
- [2] H. Richter, Z. P. Wang, L. Ley, *Solid State Commun.* **39**, 625 (1981).
- [3] I. H. Campbell, P. M. Fauchet, *Solid State Commun.* **58**, 739 (1986).
- [4] P. Milani, C. F. Bottani, *Handbook of Nanostructured materials and Nanotechnology*, Ed. H. S. Nalwa, Academic Press, 2000, vol. 2, p 213.
- [5] M. P. Chamberlain, C. Trallero-Giner, A. Debernardi, M. Cardona, *Phys. Rev. B* **51**, 1680 (1995)
- [6] C. Trallero-Giner, A. Debernardi, M. Cardona, E. Menendez-Poupin, A.I. Ekimov, *Phys. Rev. B* **57**, 4664 (1998).
- [7] J. Zi, H. Büscher, C. Falter, W. Ludwig, K. Zhang, X. Xie, *Appl. Phys. Lett.* **69**, 200 (1996).
- [8] M. I. Vasilevski, A. G. Rolo, M. J. M. Gomes, *Solid State Commun.* **104**, 381 (1997); *Microelectronic Engineering* **43-44**, 715 (1998).
- [9] A. Tanaka, S. Onary, T. Arai, *Phys. Rev. B* **45**, 6587 (1992).
- [10] Z. Iqbal, S. Veprek, *J. Phys. C: Solid State Phys.* **15**, 377 (1982).
- [11] D. R. dos Santos, I.L. Torriani, *Solid State Commun.* **85**, 307 (1993).
- [12] Ch. Ossadnik, S. Veprek, I. Gregora, *Thin Solid Films* **337**, 148 (1999).
- [13] W.S.O. Rodden, C.N. Ironside, C.M. Sotomayor Torres, *Semicond. Sci. Technol.* **9**, 1839 (1994).
- [14] L. Saviot, B. Champagnon, E. Duval, I.A. Kudriavtsev, A.I. Ekimov, *J. Non-Cryst. Solids* **197**, 238 (1996).
- [15] D. Nesheva, I.P. Kotsalas, C. Raptis, E. Vateva, *J. Non-Cryst. Solids* **224**, 283 (1998).
- [16] D. Nesheva, D. Arsova, *Phys Status Solidi (a)* **176**, R3 (1999).
- [17] D. Nesheva, I.P. Kotsalas, C. Raptis, D. Arsova, *J. Appl. Phys.*, **86**, N9 (1999).
- [18] D. Nesheva, C. Raptis, Z. Levi, I. Bineva, Z. Aneva, *Asian Journal of Physics* **9**, 289 (2000).
- [19] D. Nesheva, C. Raptis, A. Perakis, I. Bineva, Z. Aneva, Z. Levi, S. Alexandrova, H. Hofmeister, *J. Appl. Phys* **92**, 4678 (2002)
- [20] G. Scamarcio, M. Lugara, D. Manno, *Phys. Rev. B* **45**, 13792 (1992).
- [21] Y-N. Hwang, S. Shin, H.L. Park, S-H. Park, U. Kim, H.S. Jeong, E-j. Shin, D. Kim, *Phys. Rev. B* **54**, 15120 (1996).
- [22] D. Nesheva, C. Raptis, Z. Levi, *Phys. Rev. B* **58**, 7913 (1998).
- [23] U.E.H. Laheld, G.T. Einevoll, *Phys. Rev. B* **55**, 5184 (1997).